Available online at www.sciencedirect.com
SCIENCE DIRECT®
International Journal of Heat and Mass Transfer 47 (2004) 1001–1013
International Journal of HEAT and MASS TRANSFER
www.elsevier.com/locate/ijhmt

Combined radiation and convection heat transfer in a porous channel bounded by isothermal parallel plates

Prabal Talukdar, Subhash C. Mishra *,[1], D. Trimis, Franz Durst

Institute of Fluid Mechanics (LSTM), University of Erlangen-Nuremberg, Cauerstrasse, 4 D-91058 Erlangen, Germany

Received 26 November 2002; received in revised form 6 August 2003

Abstract

Combined radiation and convection heat transfer in a porous medium confined between gray isothermal parallel plates is investigated. The medium is absorbing, emitting and scattering. Cases of boundaries at temperatures higher or lower than the medium are considered. In the porous medium, the boundary effect on the fully developed laminar velocity field as proposed by Kaviany is accounted for. For various values of the extinction coefficient, the scattering albedo, the conduction–radiation parameter and the boundary emissivity, Nusselt number, temperature and heat flux distributions are found for the range of values including the extreme limits of the porous medium shape parameter (PMSP), $\gamma = (W^2\phi/K)^{1/2}$, where W is the channel width, ϕ the porosity and K the permeability. For the lower limiting value of the PMSP γ, the effect of the porous medium is negligible and the situation approaches that of Poiseuille flow. For this limiting case, results from the present work are compared with those available in the literature. For medium to high values of the PMSP γ, for the purpose of comparison, some results are presented in tabular form. Radiation is found to have a significant effect on various parameters studied. The discrete transfer method was used for the solution of the radiative part of the energy equation. An iterative finite difference scheme was used to solve the energy equation.

Keywords: Porous media; Radiation; Convection

1. Introduction

Porous media have played an important role in improving the performance of many thermal systems. In recent years, in high-temperature applications, a great deal of attention has been focused on the usage of porous media [1–9]. Apart from many other applications, porous media have been utilized for enhancement of heat transfer in coolant passages [10,11] and in thermal insulation systems [1,5]. The analysis of such systems require consideration of radiation along with conduction and/or convection.

There have been various studies of the analysis of the combined radiation and convection modes of heat transfer [12–16]. In all these analyses, the medium considered is a general fluid continuum. In some investigations [2–5], combined conduction, convection and radiation heat transfer problems in porous media have been analysed with known uniform velocity across the medium. When the porosity and permeability of the porous medium are relatively high, boundary and inertia effects come into play, and in this situation, the assumption of uniform velocity across the medium is not valid [17]. In this case, the velocity distribution near the wall is non-uniform and hence it affects the heat transfer to or from the wall [17]. This aspect of non-uniform velocity distribution near the wall has been accounted by Kaviany [17]. He obtained the solution for the velocity

* Corresponding author. Address: Department of Mechanical Engineering, Indian Institute of Technology, North Guwahati, Guwahati 781039, India. Tel.: +91-361-2691173; fax: +91-361-2690762.

E-mail address: scm_iitg@yahoo.com (S.C. Mishra).

[1] On leave from: Department of Mechanical Engineering, Indian Institute of Technology (IIT), North Guwahati, Guwahati-781039, India.

0017-9310/$ - see front matter © 2003 Elsevier Ltd. All rights reserved.
doi:10.1016/j.ijheatmasstransfer.2003.09.002

Nomenclature

C_p	specific heat at constant pressure
D_h	hydraulic diameter $= 2W$
G	incident radiant energy
i	intensity
K	permeability of the porous medium
k	thermal conductivity
M	number of intensities/rays
N	conduction–radiation parameter $= k\beta/(4\sigma T_{ref}^3)$
Nu	Nusselt number $= q_w D_h/(k(T_w - T_m))$
Pe	Peclet number $= U_m D_h/\alpha_e$
Pr	Prandtl number $= v_f/\alpha_e$
q	heat flux
Re	Reynolds number $= U_m D_h/v$
S	source function
T	dimensional temperature
U_m	mean velocity
u	x-direction velocity
v	y-direction velocity
x, y	spatial coordinates, parallel and perpendicular to the direction of flow, respectively
W	width of the channel

Greek symbols

α	polar angle
β	extinction coefficient
θ	non-dimensional temperature
θ_m	non-dimensional mean temperature $= \int_0^1 u^*\theta\, d\eta_y/U_m$
η	non-dimensional length
τ	optical thickness/depth
ϕ	porosity
Ψ	non-dimensional heat flux
ω	scattering albedo
μ	dynamic viscosity
ρ	density
σ	Stefan–Boltzmann constant
γ	porous medium shape parameter $= (W^2\phi/K)^{1/2}$
ϵ	emissivity

Subscripts

c	convective
L	length
r	radiative
ref	reference
w	wall

Superscript

$*$	non-dimensional quantities

distribution which is applicable to flow with or without a porous medium. The solution for the velocity distribution over the complete range, including the limiting case of flow with or without a porous medium, was developed by Kaviany [17] by introducing a parameter called the porous medium shape parameter (PMSP), $\gamma = (W^2\phi/K)^{1/2}$, where W is the channel width, ϕ the porosity and K the permeability. When the PMSP $\gamma \to 0$, a fully developed velocity profile for Poiseuille flow is obtained. When the PMSP $\gamma \to \infty$, the slug flow condition is achieved and, in this case, the velocity distribution is uniform. Kaviany found the Nusselt number Nu and the temperature distributions over a wide range of values of the PMSP γ. He showed that Nu for fully developed fields varies from 7.54 for $\gamma \to 0$ to 9.87 for $\gamma \to \infty$. The PMSP γ has also been found to have a significant effect on the temperature distribution. Kaviany did not consider the effect of radiation.

Chawla and Chan [12] carried out an analysis for the combined radiation and convection in thermally developing Poiseuille flow. They showed that in the presence of radiation, unlike the case of pure convection, there is no fully developed thermal field. Nu varies in the flow direction, and the radiation contribution to the total heat flux, Nu and temperature increases along the flow direction. Further, radiative parameters such as the extinction coefficient, the scattering albedo and the boundary emissivity have significant effects on heat flux, Nu and temperature. The work of Chawla and Chan [12] can be viewed as a study of convection–radiation heat transfer for the limiting case of the PMSP $\gamma \to 0$. Kaviany's work [17] can be seen as the limiting case of the convection–radiation problem with a general porous medium in which the radiation effect is negligible. In both the works, analyses were done by assuming thermo-physical properties to be constant.

After the work of Chawla and Chan [12] and Kaviany [17], many studies have been performed for different geometries [14,15,18,19]. However, none of the previous studies took into account the effect of convection and radiation for a general medium with PMSP γ, and therefore results for the variations of the Nusselt number Nu, heat flux and temperature are not available for various values of the PMSP γ. The present work was aimed at extending the work of Chawla and Chan [12] by incorporating a general medium with PMSP γ, and that of Kaviany [17] by considering the effect of radiation. The present work thus bears significance in providing more accurate predictions especially in the area of porous medium combustion where the analysis is done either by considering fluid and solid phases as a single continuum [9] or separate continua [1–8]. In all these

studies [1–9], analysis was performed for the slug flow condition.

In the present work, the effect of radiation on flow through a porous medium bounded between two isothermal parallel plates was investigated. For parameters such as extinction coefficient, scattering albedo, conduction–radiation parameter, wall emissivity, etc., *Nu*, temperature and heat flux values at different axial locations were found for various values of the PMSP γ, including the two limits $\gamma \to 0$, and ∞. For $\gamma \to 0$, results from the present work were validated against the results of Chawla and Chan [12]. When the extinction coefficient $\beta \to 0$, the radiation effect is absent, and in this case, the present problem is the same as that of Kaviany [17]. For this case, results from the present work were found to match those of Kaviany [17]. For the purpose of comparison, results are presented in both tabular and graphical forms. The discrete transfer method (DTM) [20] was used to solve the radiative part of the energy equation, and an implicit finite difference scheme was used to solve the energy equation.

2. Formulation

Consider a porous medium with uniform porosity ϕ and permeability K bounded between two gray isothermal parallel plates as shown in Fig. 1. An absorbing, emitting and scattering porous medium is embedded in a fluid with a fully developed velocity field. The fluid and the solid matrix are in local thermal equilibrium and the two phases are considered as a continuum. The density ρ, specific heat C_p and dynamic viscosity μ of the fluid are uniform and constant. The thermal conductivity k and extinction coefficient β of the fluid–solid continuum are also assumed to be uniform and constant.

By incorporating the effect of radiation, the steady-state energy equation for the fluid–solid continuum for a planar geometry [17] is modified to

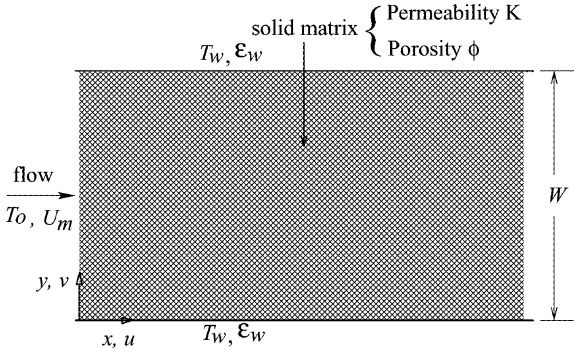

Fig. 1. Schematic diagram of the problem under consideration.

$$\rho C_p \left(u \frac{\partial T}{\partial x} + v \frac{\partial T}{\partial y} \right) = k \left(\frac{\partial^2 T}{\partial x^2} + \frac{\partial^2 T}{\partial y^2} \right) - \left(\frac{\partial q_r}{\partial x} + \frac{\partial q_r}{\partial y} \right) \tag{1}$$

where u and v are velocities parallel and perpendicular to the flow, respectively. In Eq. (1), the left-hand side is the contribution of the fluid convection, and the first and the second terms on the right-hand side represent contributions of conduction and radiation by the fluid–solid continuum, respectively. Neglecting the conductive and the radiative heat fluxes in the axial direction, for a fully developed velocity field, in non-dimensional form, Eq. (1) is written as

$$u^* \frac{\partial \theta}{\partial \eta_x} = \left(\frac{2}{Pe} \right) \frac{\partial^2 \theta}{\partial \eta_y^2} - \left(\frac{\beta W}{2NPe} \right) \frac{\partial \Psi_r}{\partial \eta_y} \tag{2}$$

where $\eta_x = x/W$ and $\eta_y = y/W$ are the non-dimensional lengths in the x and y directions, respectively, β is the extinction coefficient and W the physical thickness of the porous medium (Fig. 1). In Eq. (2), non-dimensional values of axial velocity u^*, temperature θ, Peclet number Pe, conduction–radiation parameter N, and radiative heat flux Ψ_r are defined as

$$u^* = \frac{u}{U_m}, \quad \theta = \frac{T}{T_{ref}}, \quad Pe = RePr = \left(\frac{\rho U_m D_h}{\mu} \right) \left(\frac{\mu C_p}{k} \right), \quad N = \frac{k\beta}{4\sigma T_{ref}^3}, \quad \Psi_r = \frac{q_r}{\sigma T_{ref}^4}$$

where U_m is the mean x-direction velocity, T_{ref} is some reference temperature and $D_h (= 2W)$ the hydraulic diameter.

At the entrance to the porous medium (Fig. 1), the fluid has uniform velocity U_m and temperature T_0. The temperatures of both the plates T_w are the same. For the problem under consideration, the boundary conditions in non-dimensional form are

$$\begin{aligned} &\text{Entrance } (\eta_x = 0.0): \quad v^* = 0.0, \quad u^* = 1.0, \\ &\theta = \theta_0 = \frac{T_0}{T_{ref}} \\ &\text{Solid boundaries } (\eta_y = 0.0, 1.0): \quad v^* = 0.0, \\ &u^* = 0.0, \quad \theta = \theta_w = \frac{T_w}{T_{ref}} \end{aligned} \tag{3}$$

In flows though a porous medium with relatively high porosity ϕ and permeability K, boundary and inertia effects are important, and the velocity field develops in a short distance from the entrance at a distance of the order of KU_m/ν, in contrast to a developing velocity field where no rigid matrix is present [17]. For the boundary conditions as given in Eq. (3), for flow through a porous medium with PMSP γ, the fully developed velocity profile u^* obtained by Kaviany [17] is

$$u^* = \frac{1 - e^{-2\gamma} - (1 - e^{-\gamma})\left(e^{\gamma(\eta_y - 1)} + e^{-\eta_y \gamma}\right)}{1 - e^{-2\gamma} - 2(1 - e^{-\gamma})^2 \gamma^{-1}} \tag{4}$$

It should be noted that the PMSP $\gamma = (W^2\phi/K)^{1/2}$ is the ratio of the two natural length scales, viz., the pore-particle dimension $(K/\phi)^{1/2}$ and the channel width W. When $\gamma \to 0$, the permeability $K \to \infty$, meaning that obstructions are absent from the flow field. This is the situation with fully-developed Poiseuille flow. When $\gamma \to \infty$, $K \to 0$. This is the case of a slug flow. In this situation, the boundary and the inertia effects are negligible, and the velocity profile across the porous medium is uniform. The velocity u^* profile given by Eq. (4) is applicable to all values of γ.

With the velocity distribution u^* known from Eq. (4), for the solution of the energy equation Eq. (2), information about the divergence of radiative heat $\frac{\partial \Psi_r}{\partial \eta_y}$ is required. This is obtained from

$$\frac{\partial \Psi_r}{\partial \eta_y} = 4\beta W(1 - \omega)\left[\theta^4 - \frac{G^*}{4\pi}\right] \tag{5}$$

where ω is the scattering albedo and G^* the incident radiation. If the radiation is azimuthally symmetric, which is always true for planar geometry, G^* in the DTM [21] is numerically computed from

$$G^* = \frac{G}{\frac{\sigma T_{ref}^4}{\pi}} = 2\pi \int_{\alpha=0}^{\pi} i^*(\alpha) \sin\alpha \, d\alpha \approx 2\pi \sum_{j=1}^{M} i(\alpha_j) \sin\alpha_j \sin\Delta\alpha_j \tag{6}$$

where $i^*\left(= \frac{i}{\sigma T_{ref}^4/\pi}\right)$ is the non-dimensional intensity, α the polar angle, and M the number of intensities/rays i^* considered over the complete span of $\alpha(0 \leqslant \alpha \leqslant \pi)$.

For the evaluation of G^* at any optical depth τ, the angular distribution of the intensity i^* in the DTM is found from the recursive use of the following equation:

$$i^*_{n+1} = i^*_n \exp(-\tau) + S^*[1 - \exp(-\tau)] \tag{7}$$

Eq. (7) is based on the fact that the optical distance τ between the upstream point $(n + 1)$ and the downstream point n in the ray direction α is small enough and the source function S^* given by the following equation can be assumed to be constant over the optical distance τ.

$$S^* = (1 - \omega)\theta^4 + \frac{\omega}{4\pi} G^* \tag{8}$$

For use in Eq. (7), this value of the source function is taken as equal to the average of the source function values at the upstream and downstream points.

In a ray tracing method such the DTM, rays are always traced from the boundaries to obtain the radiative information at any point in the medium. In tracing the rays, when in Eq. (7) the downstream point is next to the boundary $(n + 1 = 1)$, the upstream point is at the boundary $(n = 0)$. In this case, for the diffuse-gray boundary with emissivity ϵ_w and temperature T_w, the boundary intensity i^*_0 is found from

$$i^*_0 = \frac{\epsilon_w T_w^4}{T_{ref}^4} + 2(1 - \epsilon_w) \int_{\alpha=0}^{\pi/2} i^*(\alpha) \cos\alpha \sin\alpha \, d\alpha \approx \epsilon_w \theta_w^4 + 2(1 - \epsilon_w) \sum_{j=1}^{M/2} i^*(\alpha_j) \cos\alpha_j \sin\alpha_j \sin\Delta\alpha_j \tag{9}$$

where the first and the second terms on the right-hand side of Eq. (9) represent emitted and reflected components of the boundary intensity i^*_0, respectively.

With the intensity i^* distributions known, at any point, the non-dimensional net radiative heat flux Ψ_r is given by, and in the DTM it is numerically computed from

$$\Psi_r = 2 \int_{\alpha=0}^{\pi} i^*(\alpha) \sin\alpha \cos\alpha \, d\alpha \approx 2 \sum_{j=1}^{M} i^*(\alpha_j) \cos\alpha_j \sin\alpha_j \sin\Delta\alpha_j \tag{10}$$

To solve energy Eq. (2), the divergence of radiative heat flux given by Eq. (5) is substituted in Eq. (2), which yields the desired governing integro-differential equation to be solved:

$$u^* \frac{\partial \theta}{\partial \eta_x} = \left(\frac{2}{Pe}\right) \frac{\partial^2 \theta}{\partial \eta_y^2} - \left(\frac{2(\beta W)^2(1 - \omega)}{NPe}\right)\left(\theta^4 - \frac{G^*}{4\pi}\right) \tag{11}$$

With the radiative component known, Eq. (11) is solved using the implicit finite difference scheme in which η_x is the marching direction. For the grid independent situation, depending on the extinction coefficient β, the requirement for the control volumes has been found to be between 200 and 500. Depending on the conduction–radiation parameter N, the length increment in the axial direction has been taken between 1×10^{-6} and 1×10^{-4}. For all cases, a maximum of 64 rays has been found sufficient for the ray independent situation.

The Nusselt number Nu at the boundary is computed from

$$Nu = \frac{2}{(\theta_w - \theta_m)}\left(-\frac{\partial \theta}{\partial \eta_y} + \frac{\beta D_h}{4N} \Psi_r\right)_{\eta_y = 0.0} = Nu_c + Nu_r \tag{12}$$

where $\theta_m\left(= \frac{\int_0^1 u^* \theta \, d\eta_y}{\int_0^1 u^* \, d\eta_y}\right)$ is the bulk mean temperature of the fluid. The total Nusselt number Nu can be split as the summation of the convection Nusselt number Nu_c and the radiation Nusselt number Nu_r. It should be noted that this Nu number is different from the conventional Nu used in the study of convective heat transfer problems.

3. Results and discussion

Results for variations of the Nusselt number, temperature and heat flux are presented for both the hot-plate and the cold-plate condition. For the hot-plate condition, results for the Nusselt number and heat flux are presented in tabular form and, for the limiting case of Poiseuille flow, these are compared with the results available in the literature. All Nusselt number and heat flux values are calculated for the wall-porous medium interfaces.

It should be noted that in the absence of radiation, for both hot- and cold-plate conditions, the asymptotic value of the Nusselt number Nu is independent of the Peclet number Pe [17]. In the presence of radiation, the minimum Nu for the hot-plate condition or the asymptotic value of Nu for the cold-plate condition are independent of the Peclet number Pe. However, for low Pe the position of the minimum or the asymptotic values shift towards the entrance. When comparing results from the present work, values of Pe are taken according to the literature [12]. For other cases, Pe has been specified in the text.

3.1. Hot-plate condition

For plate temperatures higher than that of the fluid, some numerical results are presented in tabular form. For different values of the PMSP γ, these results are presented for various values of the extinction coefficient β, the scattering albedo ω, the conduction–radiation parameter N and the emissivity of the plates ϵ. The emissivities ϵ of both plates are the same. PMSP $\gamma \to 0$ represents the Poiseuille flow condition. For this limiting case, the results of the present work are validated against those of Chawla and Chan [12]. In the present study, this lower limiting value of γ is 0.1. For this case, results from the present work have been found to match those of Chawla and Chan [12].

In Tables 1–9 values of the convection Nusselt number Nu_c, the radiation Nusselt number Nu_r, the total Nusselt number Nu, the conductive heat flux Ψ_c and the radiative heat flux Ψ_r are given for $\gamma = 0.1$, 10, 100 and 300. In all these tables, numbers in the bracket are taken from [12]. All results are given for gray plates with emissivity $\epsilon = 0.5$. The Peclet number Pe corresponding to $\beta = 0.2$, 2.0, 10.0 are 0.08, 8 and 200, respectively.

It should be noted that the locations η_x in the axial direction and the values of β, ω, N and ϵ have been chosen so as to compare the results from the present work for $\gamma \to 0.0$ (which is 0.1 in this study) with those from [12]. For various values of the radiative parameters, after comparing the results for the limiting value of the PMSP γ, for the purpose of comparison with the future work, tabulated results have been provided for different values of γ.

It can be seen from Tables 1–9 that for $\gamma \to 0.0$, the results from the present work compare very well with those from [12] for Poiseuille flow.

Comparison of the results from Tables 1–9 shows that at a particular location η_x, the Nusselt number increases with decrease in the conduction–radiation parameter N. This means that when the effect of radiation increases, heat transfer is greater and as a result the Nusselt number increases. From these tables, it is also seen that with increase in the extinction coefficient β, the Nusselt number increases. Therefore, the maximum value of the Nusselt number can be found when β is high and N is low (Table 9). Further, it is seen that the value of the Nusselt number is very high near the entrance and it continues to decrease, reaches a minimum value, and then increases again. This behaviour can be explained

Table 1
Effect of the PMSP γ on Nu_c, Nu_r, Nu, Ψ_c and Ψ_r at various axial locations η_x corresponding to $\beta = 0.2$, $N = 0.01$, $\epsilon = 0.5$ and $\omega = 0.5$

η_x	γ	Nu_c	Nu_r	Nu	Ψ_c	Ψ_r
5×10^{-5}	0.1	18.2650 (18.2631)	1.4373 (1.4357)	19.7023 (19.6988)	1.7624 (1.7621)	0.1387 (0.1385)
	10	22.0936	1.4603	23.5539	2.1152	0.1398
	100	32.6706	1.5166	34.1872	3.0478	0.1415
	300	34.9135	1.5301	35.9135	3.1822	0.1416
1×10^{-3}	0.1	8.0035 (7.9930)	1.7027 (1.7010)	9.7062 (9.6940)	0.5880 (0.5868)	0.1251 (0.1249)
	10	9.1020	1.8058	10.9078	0.6376	0.1265
	100	10.8249	2.0147	12.8396	0.6845	0.1274
	300	10.9447	2.0428	12.9875	0.6820	0.1273
1×10^{-2}	0.1	7.4369 (7.4661)	4.2898 (4.2452)	11.7261 (11.7113)	0.0507 (0.0509)	0.0292 (0.0289)
	10	8.3656	4.7297	13.0953	0.0408	0.0231
	100	9.6861	5.4027	15.0888	0.0270	0.0151
	300	9.5178	5.3230	14.8407	0.0257	0.0144

Numbers in brackets are values from [12].

Table 2
Effect of the PMSP γ on Nu_c, Nu_r, Nu, Ψ_c and Ψ_r at various axial locations η_x corresponding to $\beta = 0.2$, $N = 0.1$, $\epsilon = 0.5$ and $\omega = 0.65$

η_x	γ	Nu_c	Nu_r	Nu	Ψ_c	Ψ_r
5×10^{-5}	0.1	18.3555 (18.3507)	0.1096 (0.1094)	18.4651 (18.4600)	17.7387 (17.7330)	0.1059 (0.1057)
	10	22.1614	0.1114	22.2728	21.2507	0.1068
	100	32.6992	0.1156	32.8148	30.5568	0.1080
	300	34.4083	0.1166	34.5250	31.8991	0.1081
1×10^{-3}	0.1	8.1762 (8.1765)	0.1271 (0.1267)	8.3032 (8.3032)	6.2001 (6.1998)	0.0964 (0.0961)
	10	9.2270	0.1343	9.3614	6.6866	0.0973
	100	10.8915	0.1492	11.0406	7.1546	0.0980
	300	11.0108	0.1512	11.1620	7.1320	0.0979
1×10^{-2}	0.1	7.5355 (7.5272)	0.2974 (0.2947)	7.8330 (7.8219)	0.9928 (0.9914)	0.0392 (0.0388)
	10	8.3506	0.3302	8.6807	0.8651	0.0342
	100	9.6204	0.3848	10.0052	0.6652	0.0266
	300	9.6356	0.3866	10.0222	0.6462	0.0259

Numbers in brackets are values from [12].

Table 3
Effect of the PMSP γ on Nu_c, Nu_r, Nu, Ψ_c and Ψ_r at various axial locations η_x corresponding to $\beta = 0.2$, $N = 0.5$, $\epsilon = 0.5$ and $\omega = 0.35$

η_x	γ	Nu_c	Nu_r	Nu	Ψ_c	Ψ_r
5×10^{-5}	0.1	18.3612 (18.3560)	0.0345 (0.0344)	18.3957 (18.3905)	88.7290 (88.699)	0.1665 (0.1664)
	10	22.1659	0.0350	22.2010	106.2850	0.1679
	100	32.7014	0.0364	32.7378	152.8085	0.1699
	300	34.4103	0.0367	34.4470	159.5200	0.1700
1×10^{-3}	0.1	8.1885 (8.1883)	0.0399 (0.0398)	8.2283 (8.2281)	31.1024 (31.0990)	0.1514 (0.1513)
	10	9.2370	0.0421	9.2791	33.5330	(0.1529)
	100	10.8986	0.0468	10.9454	35.8738	0.1539
	300	11.0181	0.0474	11.0655	35.7615	0.1538
1×10^{-2}	0.1	7.5503 (7.5392)	0.0923 (0.0920)	7.6426 (7.6312)	5.1385 (5.1290)	0.0628 (0.0626)
	10	8.3609	0.1024	8.4632	4.4954	0.0550
	100	9.6256	0.1192	9.7448	3.4815	0.0431
	300	9.6448	0.1197	9.7646	3.3843	0.0420

Numbers in brackets are values from [12].

Table 4
Effect of the PMSP γ on Nu_c, Nu_r, Nu, Ψ_c and Ψ_r at various axial locations η_x corresponding to $\beta = 2.0$, $N = 0.01$, $\epsilon = 0.5$ and $\omega = 0.65$

η_x	γ	Nu_c	Nu_r	Nu	Ψ_c	Ψ_r
5×10^{-4}	0.1	38.0285 (38.1617)	38.3328 (38.2953)	76.3613 (76.4570)	0.3758 (0.3784)	0.3788 (0.3771)
	10	47.7491	38.6457	86.3947	0.4709	0.3811
	100	84.3904	39.3199	123.7103	0.8264	0.3850
	300	100.5869	39.5239	140.1109	0.9817	0.3857
1.7×10^{-2}	0.1	12.1285 (12.3321)	43.1489 (43.0596)	55.2774 (55.3917)	0.0949 (0.0964)	0.3374 (0.3367)
	10	14.6493	45.3705	60.0198	0.1120	0.3468
	100	20.1548	49.5306	69.6854	0.1451	0.3566
	300	20.6410	50.1743	70.8153	0.1467	0.3567
7.5×10^{-2}	0.1	14.9881 (15.8528)	78.4209 (77.9556)	93.4089 (93.8084)	0.0419 (0.0442)	0.2192 (0.2175)
	10	17.6969	89.4096	107.1065	0.0427	0.2158
	100	22.4731	106.8565	129.3296	0.0413	0.1964
	300	22.9721	108.8939	131.8660	0.0404	0.1917

Numbers in brackets are values from [12].

Table 5
Effect of the PMSP γ on Nu_c, Nu_r, Nu, Ψ_c and Ψ_r at various axial locations η_x corresponding to $\beta = 2.0$, $N = 0.1$, $\epsilon = 0.5$ and $\omega = 0.65$

η_x	γ	Nu_c	Nu_r	Nu	Ψ_c	Ψ_r
5×10^{-4}	0.1	38.9269 (38.9057)	3.8212 (3.8174)	42.7481 (42.7232)	3.8627 (3.8604)	0.3792 (0.3788)
	10	48.4780	3.8503	52.3283	4.8016	0.3814
	100	84.7300	3.9153	88.6454	8.3333	0.3851
	300	100.5869	3.9354	104.7597	9.8833	0.3858
1.7×10^{-2}	0.1	12.4103 (12.4267)	3.8731 (3.8661)	16.2835 (16.2928)	1.1300 (1.1315)	0.3527 (0.3520)
	10	14.7206	3.9955	18.7160	1.3181	0.3578
	100	19.6965	4.2643	23.9608	1.6820	0.3642
	300	20.1436	4.3113	24.4550	1.6526	0.3636
7.5×10^{-2}	0.1	8.5077 (8.5302)	4.3560 (4.3456)	12.8637 (12.8758)	0.6337 (0.6353)	0.3245 (0.3237)
	10	9.7774	4.6207	14.3981	0.6977	0.3297
	100	11.8253	5.1447	16.9700	0.7671	0.3337
	300	11.9618	5.2149	17.1767	0.7649	0.3334
5×10^{-1}	0.1	9.1921 (9.3705)	9.6248 (9.4918)	18.8170 (18.8623)	0.1347 (0.1370)	0.1411 (0.1387)
	10	10.4825	10.7989	21.2814	0.1196	0.1232
	100	12.4876	12.7332	25.2208	0.0910	0.0928
	300	12.5015	12.8150	25.3165	0.0876	0.0898

Numbers in brackets are values from [12].

Table 6
Effect of the PMSP γ on Nu_c, Nu_r, Nu, Ψ_c and Ψ_r at various axial locations η_x corresponding to $\beta = 2.0$, $N = 0.5$, $\epsilon = 0.5$ and $\omega = 0.65$

η_x	γ	Nu_c	Nu_r	Nu	Ψ_c	Ψ_r
5×10^{-4}	0.1	39.0108 (38.9758)	0.7640 (0.7633)	39.7749 (39.7391)	19.3623 (19.3440)	0.3792 (0.3788)
	10	48.5449	0.7698	49.3147	24.0503	0.3814
	100	84.7604	0.7828	85.5431	41.6974	0.3851
	300	100.8453	0.7868	101.6321	49.4459	0.3858
1.7×10^{-2}	0.1	12.5557 (12.5587)	0.7676 (0.7662)	13.3233 (13.3249)	5.7882 (5.7893)	0.3539 (0.3532)
	10	14.8170	0.7907	15.6077	6.7201	0.3586
	100	19.7197	0.8424	20.5621	8.5375	0.3647
	300	20.1639	0.8515	21.0154	8.6398	0.3649
7.5×10^{-2}	0.1	8.5888 (8.5942)	0.8357 (0.8337)	9.4245 (9.4280)	3.3923 (3.3942)	0.3301 (0.3293)
	10	9.7817	0.8810	10.6626	3.7150	0.3346
	100	11.7250	0.9731	12.6981	4.0763	0.3383
	300	11.8564	0.9857	12.8421	4.0668	0.3381
5×10^{-1}	0.1	7.7343 (7.7450)	1.4958 (1.4868)	9.2300 (9.2318)	1.1881 (1.1893)	0.2298 (0.2283)
	10	8.6370	1.6700	10.3017	1.1435	0.2211
	100	10.0718	1.9871	12.0588	1.0214	0.2015
	300	10.1630	2.0171	12.1801	1.0033	0.1991

Numbers in brackets are values from [12].

well by Fig. 2(a) and (b). In Fig. 2(a), the effect of β on variation of the Nusselt number along the axial length η_x is shown, and in Fig. 2(b) the same is shown for the effect of N. The value of N in Fig. 2(a) is 0.1 and the value of β in Fig. 2(b) is 1.0. Both plates are black ($\epsilon = 1$) and an absorbing–emitting situation ($\omega = 0.0$) is considered in both cases. The Peclet number Pe in both cases is 20. The plots in these figures clearly explain the trends described above.

Another important finding from Tables 1–9 and Fig. 2(a) and (b) is that the value of the Nusselt number increases with increase in PMSP γ. For particular β and N, this trend is the same for all γ values. The Nusselt number reaches a maximum as the situation approaches the slug flow condition ($\gamma \to \infty$). It also indicates that with the insertion of a solid porous matrix, the heat transfer increases and with the consideration of radiation, more and more heat is transferred. In Fig. 2(a) and

Table 7
Effect of the PMSP γ on Nu_c, Nu_r, Nu, Ψ_c and Ψ_r at various axial locations η_x corresponding to $\beta = 10.0$, $N = 0.01$, $\epsilon = 0.5$ and $\omega = 0.65$

η_x	γ	Nu_c	Nu_r	Nu	Ψ_c	Ψ_r
1.25×10^{-2}	0.1	40.0834 (40.0439)	191.4109 (191.0990)	231.4943 (231.1430)	0.0777 (0.0776)	0.3708 (0.3702)
	10	47.2705	200.2732	247.5437	0.0914	0.3871
	100	79.5535	214.4573	294.0109	0.1525	0.4110
	300	93.2099	217.3074	310.5173	0.1779	0.4147
0.25	0.1	31.0859 (33.5402)	188.3844 (185.9680)	219.4703 (219.5080)	0.0367 (0.0396)	0.2227 (0.2195)
	10	34.8296	207.8403	242.6699	0.0391	0.2334
	100	40.7965	238.7365	279.5330	0.0415	0.2429
	300	41.4571	242.0937	283.5508	0.0415	0.2425
0.8375	0.1	36.6441 (76.0301)	479.6952 (439.1020)	516.3393 (515.1320)	0.0053 (0.0109)	0.0696 (0.0627)
	10	54.5008	517.2532	570.0750	0.0030	0.0576
	100	43.4243	611.1619	654.5862	0.0038	0.0376
	300	41.5927	621.1797	662.7094	0.0036	0.0361

Numbers in brackets are values from [12].

Table 8
Effect of the PMSP γ on Nu_c, Nu_r, Nu, Ψ_c and Ψ_r at various axial locations η_x corresponding to $\beta = 10.0$, $N = 0.1$, $\epsilon = 0.5$ and $\omega = 0.65$

η_x	γ	Nu_c	Nu_r	Nu	Ψ_c	Ψ_r
1.25×10^{-2}	0.1	38.2455 (38.2081)	19.7157 (19.6944)	57.9613 (57.9024)	0.7544 (0.7568)	0.3905 (0.3901)
	10	47.8008	20.1942	67.9950	0.9419	0.3992
	100	83.0224	21.1173	104.1396	1.6257	0.4143
	300	97.1288	21.3529	118.4817	1.8941	0.4172
0.25	0.1	14.7375 (14.8006)	17.0947 (17.0401)	31.8322 (31.8407)	0.2649 (0.2683)	0.3099 (0.3089)
	10	17.4104	18.3143	35.7247	0.3087	0.3274
	100	23.9488	20.4925	44.4413	0.4083	0.3517
	300	24.6617	20.7712	45.4383	0.4161	0.3527
0.8375	0.1	11.8354 (11.9335)	16.4123 (16.3170)	28.2477 (28.2505)	0.1791 (0.1821)	0.2505 (0.2490)
	10	13.4328	17.9809	31.4137	0.1965	0.2653
	100	16.3539	20.6106	36.9645	0.2210	0.2809
	300	16.5953	20.8843	37.4796	0.2210	0.2806
2.5	0.1	13.3499 (13.5552)	20.1011 (19.8900)	33.4510 (33.4452)	0.1232 (0.1257)	0.1865 (0.1844)
	10	15.0317	22.4745	37.5063	0.1267	0.1905
	100	17.9534	26.6272	44.5806	0.1268	0.1891
	300	18.2783	27.1124	45.3906	0.1262	0.1883

Numbers in brackets are values from [12].

(b), the result for $\beta = 0$ indicates the absence of radiation. The value of the Nusselt number is found to be a minimum in this case. Also, it is seen that the results for $N = 10$ almost coincide with those for $\beta = 0$. This is because, for higher values of N, the effect of radiation is lower. For $N = 10$, the effect of radiation is negligible, and situation becomes pure convection-like.

It can be seen from Fig. 2 that when the radiation effect is negligible ($\beta = 0$ in Fig. 2(a) and $N = 10$ in Fig. 2(b)), the Nusselt number reaches an asymptotic value. This is possible when the temperature profile reaches a fully developed state. In the absence of radiation, it can be interpreted from these figures that this fully developed temperature profile is achieved for all values of γ. However, with radiation a fully developed temperature profile is not obtained and, therefore, an asymptotic value of the Nusselt number is not achieved for any value of γ. This behaviour is consistent with the findings of previous work [12,15] for Poiseuille flow ($\gamma \to 0$).

As mentioned above, the trend of the developing temperature profile, can be clearly understood from Fig. 3(a) and (b) where at four axial locations η_x, similarity temperature profiles $((\theta_w - \theta)/(\theta_w - \theta_m))$ are drawn from the centreline ($\eta_y = 0.5$) to the plate ($\eta_y = 1$). Fig.

Table 9
Effect of the PMSP γ on Nu_c, Nu_r, Nu, Ψ_c and Ψ_r at various axial locations η_x corresponding to $\beta = 10.0$, $N = 0.5$, $\epsilon = 0.5$ and $\omega = 0.65$

η_x	γ	Nu_c	Nu_r	Nu	Ψ_c	Ψ_r
1.25×10^{-2}	0.1	38.8602 (38.8142)	3.9545 (3.9496)	42.8147 (42.7639)	3.8528 (3.8513)	0.3924 (0.3919)
	10	48.3675	4.0420	52.4095	4.7871	0.4003
	100	83.4446	4.2178	87.6624	8.1987	0.4146
	300	97.5544	4.2640	101.8184	9.5435	0.4175
0.25	0.1	14.5551 (14.5670)	3.5020 (3.4932)	18.0571 (18.0602)	1.3641 (1.3677)	0.3288 (0.3280)
	10	17.3984	3.6896	21.0879	1.6110	0.3422
	100	24.2549	4.0504	28.3053	2.1640	0.3619
	300	25.0294	4.1032	29.1326	2.2103	0.3628
0.8375	0.1	10.3223 (10.3334)	3.3320 (3.3186)	13.6543 (13.6520)	0.8843 (0.8872)	0.2861 (0.2849)
	10	11.9906	3.5732	15.5637	1.0011	0.2990
	100	15.1114	4.0052	19.1166	1.1817	0.3138
	300	15.3448	4.0568	19.4016	1.1846	0.3138
2.5	0.1	8.4760 (8.4963)	3.3994 (3.3797)	11.8754 (11.8761)	0.5908 (0.5935)	0.2375 (0.2361)
	10	9.5688	3.7045	13.2733	0.6332	0.2457
	100	11.3123	4.2286	15.5410	0.6704	0.2512
	300	11.4532	4.2873	15.7404	0.6680	0.2506

Numbers in brackets are values from [12].

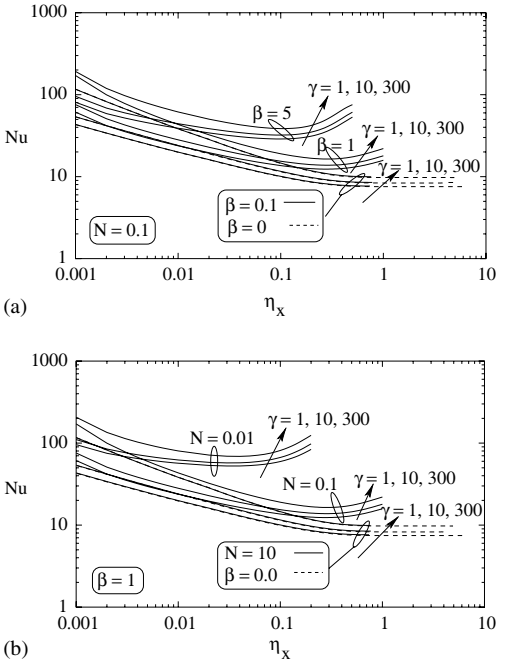

Fig. 2. Variation of the total Nusselt number Nu along the axial length η_x for various values of PMSP γ: (a) effect of the extinction coefficient β; (b) effect of the conduction–radiation parameter N. Results for Nu without radiation effect ($\beta = 0$) are also shown.

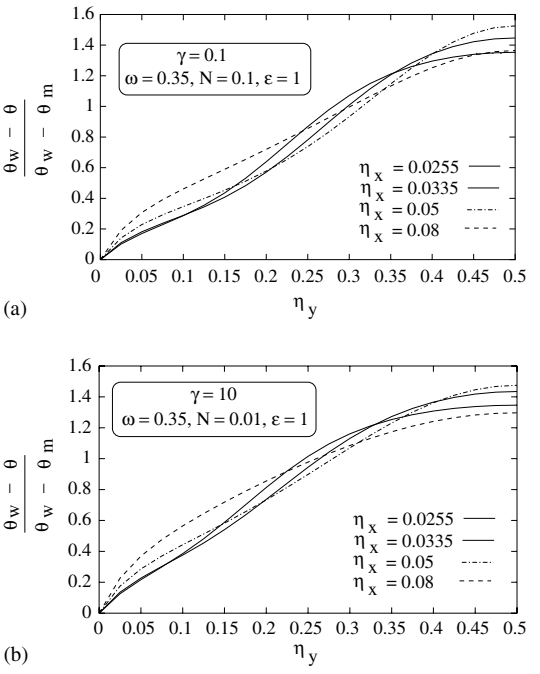

Fig. 3. Similarity temperature profile $\frac{\theta_w-\theta}{\theta_w-\theta_m}$ at different axial locations: (a) $\gamma = 0.1$ and (b) $\gamma = 10$, corresponding to $\beta = 2$, $\omega = 0.35$, $N = 0.01$, $\epsilon = 1$ and $Pe = 8.0$.

3(a) represents the situation of Poiseuille flow ($\gamma = 0.1$), whereas Fig. 3(b) is a case of flow through a porous medium with PMSP $\gamma = 10$. These two figures clearly indicate that irrespective of the value of PMSP γ, in the presence of radiation, a fully developed temperature profile does not occur.

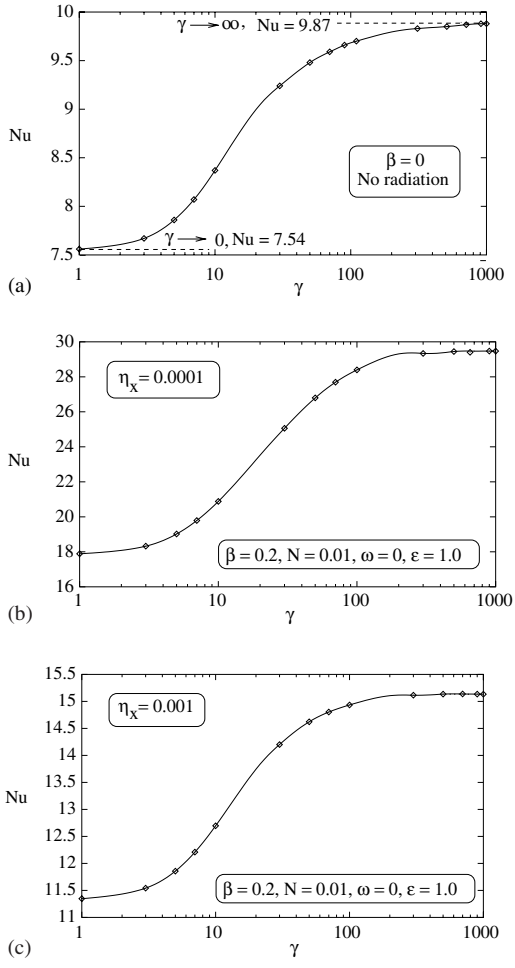

Fig. 4. Variation of the total Nusselt number Nu with PMSP γ: (a) without radiation ($\beta = 0.0$), (b) with radiation at axial location $\eta_x = 0.0001$ and (c) with radiation at axial location $\eta_x = 0.001$; $Pe = 0.08$.

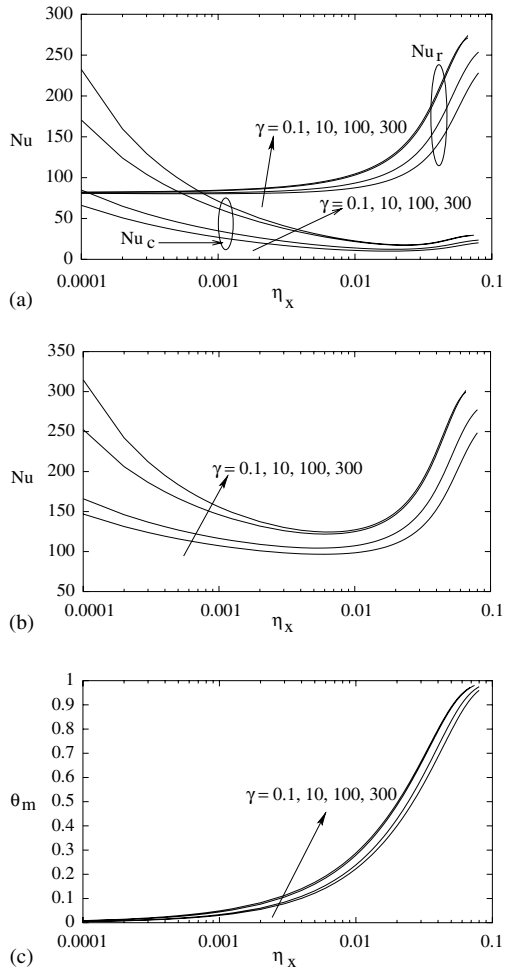

Fig. 5. Effect of PMSP γ on variations of (a) convection Nusselt number Nu_c and radiation Nusselt number Nu_r, (b) total Nusselt number Nu and (c) bulk-mean temperature θ_m along the axial distance η_x; $\beta = 2.0$, $\omega = 0.35$, $\epsilon = 1.0$, $N = 0.01$ and $Pe = 8.0$.

The increase in the Nusselt number with PMSP γ is shown in Fig. 4. For the results shown in Fig. 4(a), the radiation effect is absent. The Nusselt number values represented by the plot in Fig. 4(a) are the asymptotic values found from the fully developed temperature fields. This plot has been provided to show the correctness of the results from the present work. The minimum value of the Nusselt number (7.54) corresponds to $\gamma = 0.1$ (Poiseuille flow) and the maximum value of 9.87 is found at $\gamma = 1000$ (slug flow). These values are identical with those found by Kaviany [17]. Since with radiation there is no asymptotic value of the Nusselt number, in Fig. 4(b) and (c) Nu variations with γ are shown at two different axial locations, $\eta_x = 0.0001$ and 0.001. In both the figures, at different η_x, the trend for the variation of Nu with γ is similar to that without radiation (Fig. 4(a)). With increase in PMSP γ, the Nusselt number changes, and at different η_x, the trends are similar.

The effects of the PMSP γ on the convection Nusselt number Nu_c, the radiation Nusselt number Nu_r, the total Nusselt number Nu and the bulk mean temperature θ_m are shown in Fig. 5(a)–(c). The variations of Nu_c and Nu_r in Fig. 5(a) explain the trends of the variation of Nu in Fig. 5(b). It can be seen from Fig. 5(a) that effect of radiation increases as the distance from the entrance ($\eta_x = 0.0$) increases. Nu_r increases very sharply in the later part of the axial length and, as a result, the total Nusselt number Nu increases again after it has reached a minimum value. With increase in γ, the values of Nu_c, Nu_r and Nu increase. The effect of γ on Nu_c is maximum at the entrance and it decreases as the distance from the

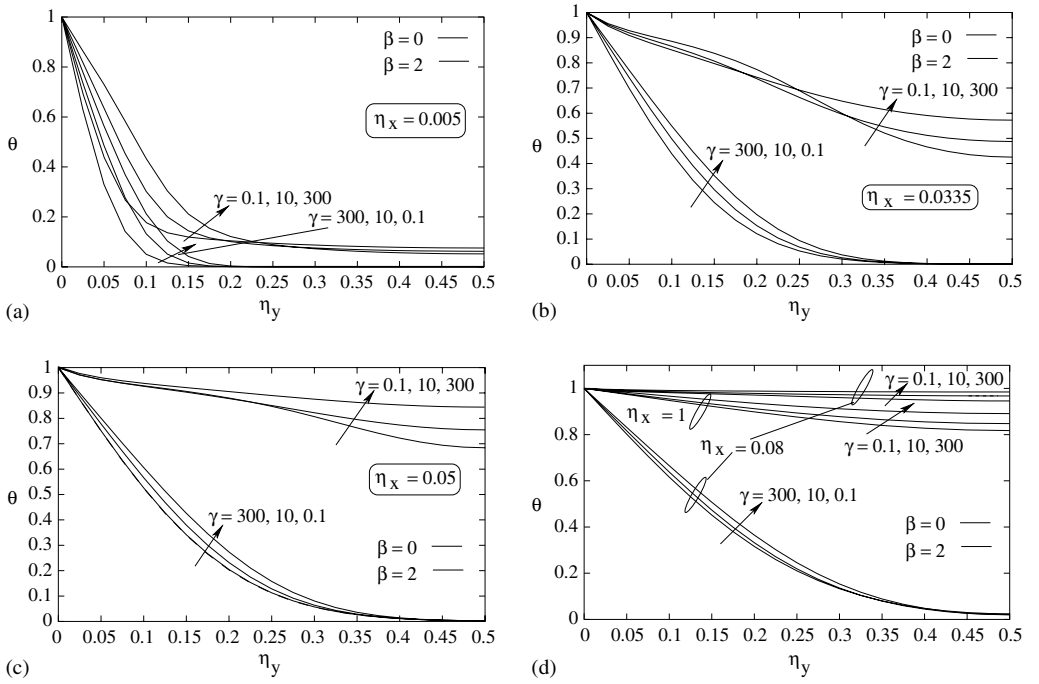

Fig. 6. Effect of PMSP γ on variation of temperature θ normal to the flow direction at axial locations: (a) $\eta_x = 0.005$, (b) $\eta_x = 0.0335$, (c) $\eta_x = 0.05$ and (d) $\eta_x = 0.08$ and 1.0; $\omega = 0.35$, $N = 0.01$ and $\epsilon = 1$; $Pe = 8.0$. Results without radiation effect ($\beta = 0$) are also shown.

entrance increases. In Fig. 4(c), the effect of γ on the bulk mean temperature θ_m is shown. It can be seen that θ_m increases with η_x and also that with increase in γ, θ_m increases.

The effect of the PMSP γ on temperature θ distributions along the channel width at different axial locations η_x are plotted in Fig. 6. In Fig. 6(a)–(d), the η_x values are 0.005, 0.0335, 0.05 and 0.8, respectively. To demonstrate the effect of radiation ($\beta = 2.0$), the results without radiation ($\beta = 0.0$) are also considered. In Fig. 6(d), θ profiles are presented at two η_x locations, viz. $\eta_x = 0.08$ and 1.

It can be seen from Fig. 6(a)–(d) that with radiation ($\beta = 2.0$), at a given axial location η_x, the fluid temperature is closer to the plate temperature than in the case without radiation ($\beta = 0.0$). In Fig. 6(d), for $\beta = 2.0$ and $\eta_x = 0.08$, the fluid temperature is closer to the plate temperature than for $\beta = 0.0$ at $\eta_x = 0.08$ and 1.0. This clearly shows the high rate of heat transfer due to radiation. For $\beta = 0.0$ (without radiation), (Fig. 6(a)–(c)), the temperature decreases with increase in γ close to the entrance, but far from the entrance ($\eta_x = 1.0$), the opposite trend is observed (Fig. 6(d)). However, in the presence of radiation ($\beta = 2.0$), the temperature always increases with increase in γ at all axial locations.

3.2. Cold-plate condition

In Figs. 7 and 8, results for plate temperatures lower than the fluid temperature are provided.

For various values of PMSP γ, the effects of β and N on the total Nusselt number Nu are shown in Fig. 7(a) and (b), respectively. For $\omega = 0.0$, $\epsilon = 1.0$, and $Pe = 20$, in Fig. 7(a), results are shown for $N = 0.1$, and in Fig. 7(b) results are given for $\beta = 1$. Unlike the cases with heating (Fig. 2(a)–(b)), in the present case of cooling, the Nusselt number reaches an asymptotic value. This trend for all values of the PMSP γ is consistent with the earlier work of Azad and Modest [22] for the cold condition of gas-particulate tube flow ($\gamma \to 0.0$). Like before, Nu is higher for higher values of γ, and when $\beta \to 0.0$ (Fig. 7(a)) or N becomes high (Fig. 7(b)), the effect of radiation becomes negligible, and Nu for these cases approach the Nu values obtained without radiation. Furthermore, the Nusselt number is found to be higher for lower values of N and higher values of β.

Results for the effects of γ on variations of Nu_c, Nu_r, Nu and the bulk-mean temperature θ_m are given in Fig. 8(a)–(c). Unlike the case of heating (Fig. 5), the radiation effect is found to be maximum at the entrance and decreases downstream. Accordingly, Nu_r decreases along the axial length and reaches an asymptotic value. With

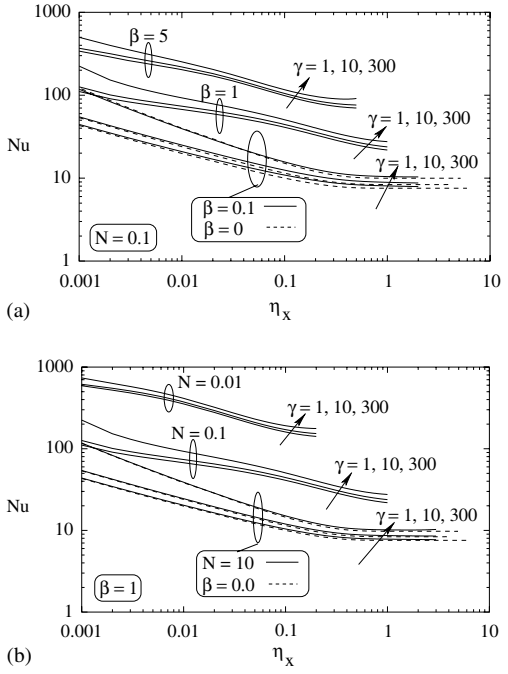

Fig. 7. Variation of the total Nusselt number Nu along the axial length η_x for various values of PMSP γ: (a) effect of the extinction coefficient β and (b) effect of the conduction–radiation parameter N. Results for Nu without radiation effect ($\beta = 0$) are also shown.

increase in γ, both the Nusselt number and θ_m increase. However, θ_m decreases along the axial length η_x.

4. Conclusions

With the insertion of a porous solid matrix, heat transfer is significantly enhanced. Both the radiation Nusselt number and the convection Nusselt number increase with increase in PMSP γ. The behaviour of the total Nusselt number for all values of PMSP γ is found to be the same as that for the combined radiative and convective heat transfer in Poiseuille flow ($\gamma \to 0.0$). For the hot-plate condition, the Nusselt number decreases along the axial length, reaches a minimum value and then increases again. For the cold-plate condition, the total Nusselt number decreases along the axial length and reaches an asymptotic value. For the hot-plate condition, the effect of γ on the radiation Nusselt number is smaller near the entrance region, but it increases along the axial length. The opposite is the case with the convection Nusselt number. For the cold-plate condition, the effect of γ decreases gradually in the streamwise direction. In the presence of radiation, a fully developed temperature field is not obtained. In the limiting cases of $\gamma \to 0.0$ and $\beta = 0.0$, the results from the present work were found to match those available in the literature.

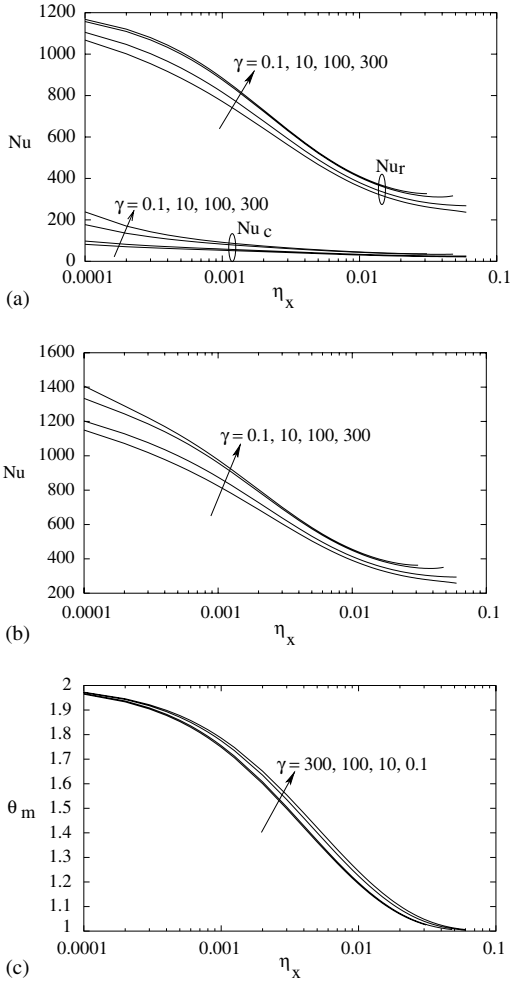

Fig. 8. Effects of PMSP γ on variations of (a) convection Nusselt number Nu_c and radiation Nusselt number Nu_r, (b) total Nusselt number Nu and (c) bulk-mean temperature θ_m along the axial distance η_x; $\beta = 2.0$, $\omega = 0.35$, $\epsilon = 1.0$, $N = 0.01$ and $Pe = 8.0$.

Acknowledgements

The second author (SCM) received support for this work through a Research Fellowship of the Alexander von Humboldt Foundation.

References

[1] K.Y. Wang, C.L. Tien, Thermal insulation in flow systems: combined radiation and convection through a porous segment, J. Heat Transfer 106 (1984) 453–459.

[2] S.W. Baek, The premixed flame in a radiatively active porous medium, Combust. Sci. Technol. 64 (1989) 277–287.
[3] H. Yoshida, J.H. Yun, R. Echigo, Transient characteristics of combined conduction, convection and radiation heat transfer in porous media, Int. J. Heat Mass Transfer 33 (5) (1990) 847–857.
[4] T.W. Tong, S.B. Sathe, Heat transfer characteristics of porous radiant burners, J. Heat Transfer 113 (1991) 423–428.
[5] S. Maruyama, T. Aihara, R. Viskanta, Transient behaviour of an active thermal protection system, Int. J. Heat Mass Transfer 34 (3) (1991) 625–632.
[6] D. Trimis, F. Durst, Combustion in a porous medium—advances and applications, Combust. Sci. Technol. 121 (1996) 153–168.
[7] M.A. Hossain, M.A. Alim, D.A.S. Rees, Effect of radiation on free convection from a porous vertical plate, Int. J. Heat Mass Transfer 42 (1999) 181–191.
[8] A.A. Mohammadien, M.F. El-amin, Thermal dispersion–radiation effects on non-Darcy natural convection in a fluid saturated porous medium, Transport Porous Media 40 (2000) 153–163.
[9] G. Brenner, K. Pickenacker, O. Pickenacker, D. Trimis, K. Wawrzinek, T. Weber, Numerical and experimental investigations of matrix-stanilized methane/air combustion in inert porous media, Combust. Flame 123 (1/2) (2000) 201–213.
[10] J.C.Y. Koh, R. Colony, Analysis of cooling effectiveness for porous material in a coolant passage, J. Heat Transfer 96 (1974) 324–330.
[11] J.C.Y. Koh, R.L. Stevens, Enhancement of cooling effectiveness by porous material in coolant passages, J. Heat Transfer 97 (1975) 309–311.
[12] T.C. Chawla, S.H. Chan, Combined radiation convection in thermally developing Poiseuille flow with scattering, J. Heat Transfer 102 (1980) 297–307.
[13] M. Hirano, T. Miyauchi, Y. Takahira, Enhancement of radiative heat transfer in the laminar channel flow of non-gray gases, Int. J. Heat Mass Transfer 31 (2) (1988) 367–374.
[14] T.K. Kim, H.S. Lee, Two-dimensional anisotropic scattering radiation in a thermally developing Poiseuille flow, J. Thermophys. Heat Transfer 4 (3) (1990) 292–298.
[15] M. Kassemi, B.T.F. Chung, Two-dimensional convection and radiation with scattering from a Poiseuille flow, J. Thermophys. Heat Transfer 4 (1) (1990) 98–105.
[16] W.M. Yan, H.Y. Li, Radiation effects on mixed convection heat transfer in a vertical square duct, Int. J. Heat Mass Transfer 44 (7) (2001) 1401–1410.
[17] M. Kaviany, Laminar flow through a porous channel bounded by isothermal parallel plates, Int. J. Heat Mass Transfer 28 (4) (1985) 851–858.
[18] J.S. Chiou, Combined radiation–convection heat transfer in a pipe, J. Thermophys. Heat Transfer 7 (1) (1993) 178–180.
[19] C.K. Krishnaprakas, K. Badari Narayana, P. Dutta, Combined convective and radiative heat transfer in turbulent tube flow, J. Thermophys. Heat Transfer 13 (3) (1999) 390–394.
[20] N.G. Shah, New Method of Computation of Radiation Heat Transfer in Combustion Chambers. PhD Thesis, Imperial College, University of London, England, 1979.
[21] P. Talukdar, S.C. Mishra, Analysis of conduction–radiation problem in absorbing–emitting and anisotropically scattering media using the collapsed dimension method, Int. J. Heat Mass Transfer 45 (2002) 2159–2168.
[22] F.H. Azad, M.F. Modest, Combined radiation and convection in absorbing, emitting and anisotropically scattering gas-particulate tube flow, Int. J. Heat Mass Transfer 24 (1981) 1681–1698.